Brain Lesion Detection in 3D PET Images Using Max-Trees and a New Spatial Context Criterion

Hélène Urien[1(✉)], Irène Buvat[2], Nicolas Rougon[3], Michaël Soussan[2], and Isabelle Bloch[1]

[1] LTCI, Télécom ParisTech, Université Paris-Saclay, 75013 Paris, France
helene.urien@telecom-paristech.fr
[2] IMIV, Inserm, CEA, Université Paris-Sud, CNRS, Université Paris-Saclay, 91400 Orsay, France
[3] MAP5, CNRS, Télécom SudParis, Université Paris-Saclay, 91011 Evry, France

Abstract. In this work, we propose a new criterion based on spatial context to select relevant nodes in a max-tree representation of an image, dedicated to the detection of 3D brain tumors for ^{18}F-FDG PET images. This criterion prevents the detected lesions from merging with surrounding physiological radiotracer uptake. A complete detection method based on this criterion is proposed, and was evaluated on five patients with brain metastases and tuberculosis, and quantitatively assessed using the true positive rates and positive predictive values. The experimental results show that the method detects all the lesions in the PET images.

Keywords: Max-tree representation · Spatial context · Brain tumors · Positron Emission Tomography · Detection

1 Introduction

Automatic tumor detection in Positron Emission Tomography (PET) imaging, usually performed as a first step before segmentation, is a difficult task due to the coexistence of physiological and pathological radiotracer uptake, both resulting in a high signal intensity. For example, in ^{18}F-FDG PET imaging, the distinction between brain metastases and the whole physiological brain uptake is not obvious, especially for small lesions. In clinical routine, the detection problem is overcome by manually defining a volume surrounding the tumor. The segmentation is then performed within this volume of interest using various strategies [1].

In a multimodal segmentation process, combining PET with an anatomical modality, such as Magnetic Resonance Imaging (MRI), tumor detection can also turn to be a critical initialization step to assess the location and number of lesions, and so influences the final result. A typical initialization method consists in thresholding the PET signal intensity, which can be further refined using mathematical morphology [2]. However, using such a threshold as a detection step has two main limitations. First, it is not adapted to patients having several lesions of different metabolisms, and can lead to an under- or over-detection

J. Angulo et al. (Eds.): ISMM 2017, LNCS 10225, pp. 455–466, 2017.
DOI: 10.1007/978-3-319-57240-6_37

according the threshold value. Secondly, the use of a PET threshold does not prevent the detected tumor from merging with adjacent structures of physiological uptake, such as basal nuclei or other brain regions when using ^{18}F-FDG as a radiotracer. Thus, our goal was to design a detection method for brain PET images, providing lesion markers for a subsequent PET-MR segmentation, and detecting all the pathological areas of increased uptake, while preventing them from merging with regions with physiologically increased uptake.

In this context, we propose a method to detect brain tumors on PET images, embedding spatial context information about the tumor in a hierarchical approach. We designed a new criterion to select relevant nodes in a max-tree representation, based on contextual information modeling reasonable hypotheses about the appearance of tumors in PET images. We first describe the tumor detection method, which prevents the tumor from merging with nearby physiological uptake. Then, we show and discuss the results, which will further be used as an initialization step to our previous segmentation method performed on MRI and guided by PET information [3].

2 Proposed Detection Method

The max-tree, as used in [4], is a hierarchical representation of an image based on the study of its intensity thresholds. It can be built according to various methods (see e.g. [5,6] for a comparison). Regions of interest are then selected according to a given criterion. Since PET image threshold is a common method for tumor segmentation [1], and since the max-tree representation highlights bright areas in an image, and so potential tumors, it has already been used on PET images for tumor segmentation, for example using a shape criterion [7]. In addition, other criteria have been evaluated in hierarchical approaches, such as spatial context [8]. In this paper, we propose a new spatial context criterion applied on a max-tree representation of the image to detect potential tumors in PET images. The detection results are then refined using topological and symmetry information.

2.1 3D Hierarchical Tumor Detection Using Spatial Context Information

In our method, the max-tree representation of the PET image is computed on the SUV, and leads to a hierarchical representation of its flat zones (identified by a letter in Fig. 1a), that are homogeneous regions of unique intensity value (identified by a number in Fig. 1a). The SUV (Standardized Uptake Value) is a standardization of the PET image widely used for quantification purposes [9], which measures the tumor metabolism and depends of parameters proper to the exam (duration and radiotracer) and the patient (weight). Formally, let Ω be the spatial domain (here $\mathbb{Z}^3$ for discrete formulation). An image is defined as a function I from Ω into $\mathbb{N}$ of $\mathbb{R}^+$. The max-tree of image I is a hierarchical representation of the connected components of all its upper level sets L_n^+, namely

$L_n^+(I) = \{x \in \Omega \mid I(x) \geq n\}$, given $n \in \mathbb{N}$, within a defined neighborhood. The tree is composed of nodes, associated to the previous connected components, and edges, embedding the inclusion relation between them. A node N is said to be a descendant of a node M if a path in the tree allows linking them and if N is at a higher position in the tree than M (for example nodes F, E, D and C are descendants of node B in Fig. 1a). Inversely, M is said to be an ancestor of node N. In this paper, a node N is said to be a direct descendant of a node M if N is a descendant of M that is directly connected to it in the tree (for example nodes D and E are the direct descendants of node C in Fig. 1a).

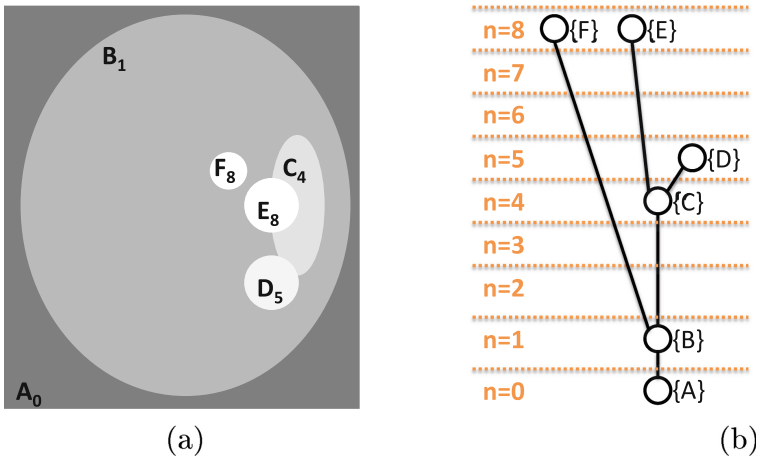

Fig. 1. A synthetic image (a) and its max-tree (b). A flat zone R_n in (a) is represented by a node R at level n in (b).

To simplify the notations, we will use the notation N both for a node of the max-tree and the corresponding region in Ω. The set of all the nodes is denoted by $MT(I)$. Let $DD(N)$ be the set of direct descendant nodes of N, $DD(N) = \{N^i, i \in I(N)\}$, with $I(N)$ the index set of the direct descendants of N. We also define $D(N)$ and $A(N)$, respectively the set of descendant and ancestor nodes of N. Let $\widehat{N}$ be the region made of the node N and all its descendant nodes $D(N)$: $\widehat{N} = N \cup D(N)$. Finally, $|N|$ denotes the number of voxels of node N, *i.e* its volume in Ω.

Once the tree is created, relevant nodes are selected according to a given criterion. We expect tumors to correspond to some of the leaf nodes. However, the distinction between nearby physiological and pathological radiotracer uptake is difficult. We propose to first apply a criterion χ_t preventing a tumor node from merging with a node including physiological uptake. We base this criterion on two hypotheses. First, an acceptable merge should result in a node having several direct descendant nodes, and a large difference in volume compared to at least one of them. We thus design the following criterion χ_t^1, taking values in $[0, 1]$:

$$\chi_t^1(N) = \max_{N^i \in DD(N)} \frac{\left|\widehat{N}\right| - \left|\widehat{N^i}\right|}{\left|\widehat{N}\right|} \tag{1}$$

Moreover, the merge does not concern too voluminous nodes, associated with almost all both physiological and pathological radiotracer uptake. The resulting criterion χ_t^2 is then designed as follows:

$$\chi_t^2(N) = e^{-\left(\frac{|\widehat{N}|}{K_t|I_b|}\right)^2} \tag{2}$$

where K_t is a positive parameter and I_b the binary mask of the brain, created by thresholding the PET image converted into SUV. The final criterion χ_t combines the two previous criteria in a conjunctive way:

$$\chi_t(N) = \chi_t^1(N)\chi_t^2(N) \tag{3}$$

The criterion χ_t is applied only to nodes having several direct descendant nodes, called merged nodes in this paper (B and C in Fig. 1a). The process for node selection based on χ_t is iterative, and promotes nodes having a high χ_t value (Algorithm 1). Among these merged nodes, the one with maximal χ_t value (node C depicted in red in Fig. 2a) and all its ancestors (crossed nodes A and B in Fig. 2a) are removed from the tree. Its descendants are kept (E and D in Fig. 2a), but not taken into account for the next search of the maximum χ_t value. This process is repeated until there is no more merged nodes to process (the only remaining node is F in Fig. 2a, which stops the search).

Algorithm 1. Node selection using χ_t

Input: I, $k = 0$, $MT^k = MT$
Output: MT (filtered max-tree according to χ_t)
  while $\exists N \in MT^k \mid |DD(N)| \geq 2$ **do**
    $k = k + 1$
    $N^k = \underset{N||DD(N)|\geq 2}{\arg\max}\ \chi_t(N)$
    $MT^k = MT^{k-1} \setminus \{N^k \cup A(N)\}$
  end while
  $MT = MT^k$

After applying the χ_t criterion, we define a context criterion χ_c for tumor detection. The spatial context volume is defined by using the distance transform of $\widehat{N}$, associating to each voxel x of the PET volume the value $D_{\widehat{N}}(x) = \min_{y \in \widehat{N}} d(x, y)$, where y is a voxel included in $\widehat{N}$, and d is the distance between two voxels (the Euclidian distance was used in this work). The context volume $C_{\widehat{N}}$ is obtained by thresholding this function, which can be formally written as $C_{\widehat{N}} = \{x \mid 0 < D_{\widehat{N}}(x) \leq s\}$, where s is a positive value. Finally, the PET image is thresholded within the spatial context volume using Otsu's method [10], to exclude white matter.

The χ_c criterion design follows three hypotheses. First, the intensity of the tumor in the PET image should be higher than the one of its surroundings. This

is embedded in the criterion χ_c^1, which should be greater than one for nodes associated to tumors:

$$\chi_c^1(N) = \frac{\mu(I_{\text{PET}}, \widehat{N})}{\mu(I_{\text{PET}}, C_{\widehat{N}})} \tag{4}$$

where $\mu(I_{\text{PET}}, V)$ is the mean intensity value of the PET image I_{PET} inside volume V, $C_{\widehat{N}}$ the context volume.

Then, the tumor should not be too voluminous. In fact, some voluminous nodes, associated to almost all pathological and physiological radiotracer uptake, can have a χ_c^1 value greater than one. The criterion χ_c^2 prevents from this situation:

$$\chi_c^2(N) = e^{-\left(\frac{|\widehat{N}|}{K_c^1 |I_b|}\right)^2} \tag{5}$$

where K_c^1 is a positive parameter.

Finally, the tumor should not be too small. The criterion χ_c^3 embedds this last hypothesis:

$$\chi_c^3(N) = \frac{K_c^2}{\left|\widehat{N}\right|} \tag{6}$$

where K_c^2 is a positive parameter.

The context criterion χ_c is then created by combining the three previous criteria, for each node $N \in MT$:

$$\chi_c(N) = \chi_c^1(N)\chi_c^2(N) - \chi_c^3(N) \tag{7}$$

The product of $\chi_c^1(N)$ and $\chi_c^2(N)$ is less than 1 for a voluminous node N, even if $\chi_c^2(N) \geq 1$. Substracting $\chi_c^3(N)$, increasing if $\left|\widehat{N}\right|$ decreases, from $\chi_c^1(N)\chi_c^2(N)$ allows having a final $\chi_c(N)$ value less than 1 for a node N of too small volume. Thus, only the nodes with a χ_c value greater than 1 are taken into account in the node selection process leading to the binary image of the detected tumors T (Algorithm 2).

The nodes maximizing the χ_c value are then selected. Among the nodes kept after the χ_t process (D, E and F in Fig. 2b), only the nodes with a value greater than 1 are considered. Among these nodes, the one of maximum χ_c value is selected, and its descendants and ancestors are removed. This process is repeated until there is no node of χ_c value greater than 1 to process. Each selected node is filled with its descendant nodes, which gives the signal intensity-based detection, shown in red in Fig. 2c.

Thus, the aim of our method is twofold: removing nodes embedding both pathological and physiological uptake, and then selecting only the tumors among the remaining nodes.

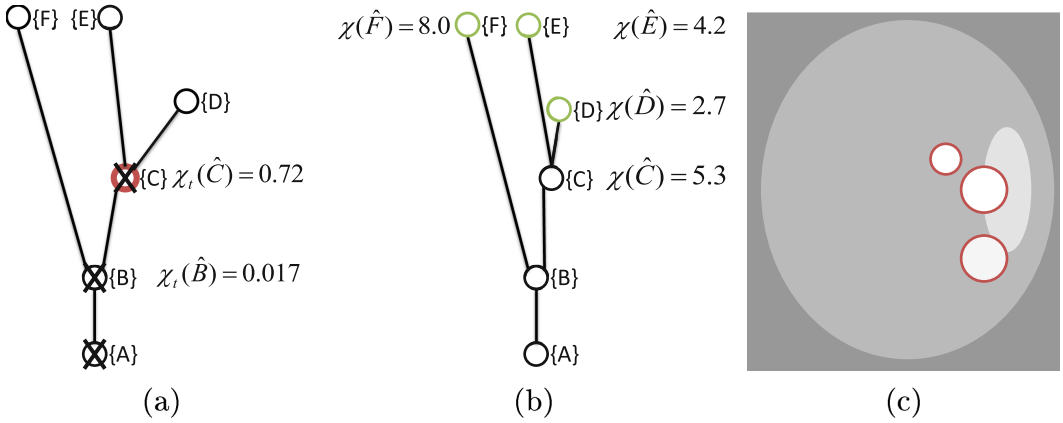

Fig. 2. Node selection process. (a) Assignment of a χ_t value to each merged node. The node of maximal χ_t value is depicted in red. The nodes and their ancestors coming from a too large node merging are not taken into account for further process (crossed nodes). (b) Assignment of a χ_c value to nodes accepted after applying the criterion χ_t (in green). (c) Contours of the resulting segmentation (in red). (Color figure online)

Algorithm 2. Node selection using χ_c

Input: I, $k = 0$, $MT^k = \{N \mid N \in MT \wedge \chi_c(N) \geq 1\}$, $T^k = \emptyset$
Output: T (selected nodes)
  while $MT^k \neq \emptyset$ **do**
    $k = k + 1$
    $N^k = \arg\max_{N \in MT^k} \chi_c(N)$
    $MT^k = MT^{k-1} \setminus \{N^k \cup A(N) \cup D(N)\}$
    $T^k = T^{k-1} \cup \{N^k \cup D(N)\}$
  end while
  $T = T^k$

2.2 Refinement Using Topological and Symmetry Information

Once the detection is obtained using the max-tree approach, we study each of the detected lesions to remove false positives due to physiological radiotracer uptake, using topological and symmetry hypotheses. First, we keep the detected lesions having only one connected component (8-connectivity) by slice. Then, based on the hypothesis that the PET signal is higher in the tumor than its symmetrical region, we compute for the remaining lesions the ratio between the mean intensity of the PET within the lesion and the mean intensity of the PET in the symmetrical region of the lesion with respect to the inter-hemispheric plane, which is automatically identified using the method from [11]. The symmetrical region is thresholded via Otsu's method [10], to exclude white matter. The set of obtained ratio values that are greater than 1 is divided into two classes (using k-means algorithm), and only the one corresponding to the highest values is kept.

3 Experimental Results

3.1 Patient Data

The proposed method was evaluated on images from 5 patients having brain lesions (tuberculosis for patient P2, and metastasis for the others), who underwent a whole body PET-MR scan. The exam was performed with a PET/MR

Table 1. Quantitative comparison between automatic lesion detections with or without post-processing (PP). The True Positive Rate (TPR) and Positive Predictive Value (PPV) are computed for each patient, before and after (TPR-PP and PPV-PP) post-processing.

Patient	P1	P2	P3	P4	P5	$\mu \pm \sigma$
TPR	1.00	1.00	1.00	1.00	1.00	1.00 ± 0.00
TPR-PP	1.00	1.00	1.00	1.00	1.00	1.00 ± 0.00
PPV	0.09	0.12	0.11	0.08	0.09	0.09 ± 0.02
PPV-PP	1.00	0.40	0.33	0.50	0.50	0.55 ± 0.23

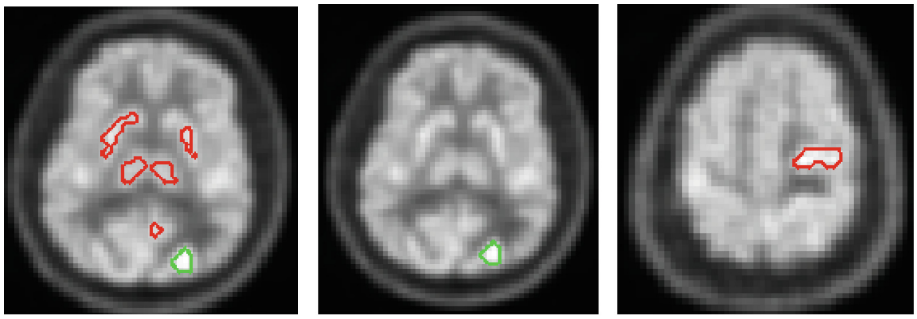

(a) (b) (c)

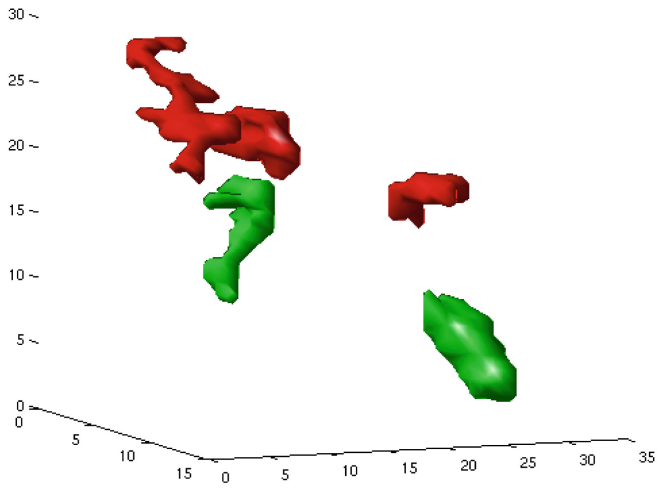

(d)

Fig. 3. Evaluation of the PP for P2: comparison between the detected lesions, true (in green) and false (in red) positives. Results shown on PET slices before (a) and after ((b) and (c)) PP, and in 3D after applying PP (d). (Color figure online)

scanner (GE SIGNA) after an initial injection of 320 MBq ^{18}F-FDG and about 100 min delay between injection and PET/MR acquisition. The voxel size in the PET images is $3.12 \times 3.12 \times 3.78\,\text{mm}^3$.

3.2 Hyperparameter Setting

The 3D 6-connectivity was used to define the connected flat zones in the SUV image and create the max-tree, and to differentiate the detected lesions while applying the post-processing. The parameter in the criterion χ_t was set to $K_t = 0.5$, while those of the spatial context criterion χ_c were set to $K_c^1 = 0.5$ and $K_c^2 = 4$. The spatial context parameter was set to $s = 1$ voxel. These hyperparameters were set experimentally to reduce the number of detected lesions for the patients having the smallest tumors (P1 and P3), and then applied to all the dataset.

3.3 Results

The ground truth PET brain lesions were those visually detected by a medical expert using only the PET data. For each patient, the computational time for the whole process (brain mask creation, lesion detection and post-processing) was about 3 min limiting the detection to a brain mask containing about 53000 voxels.

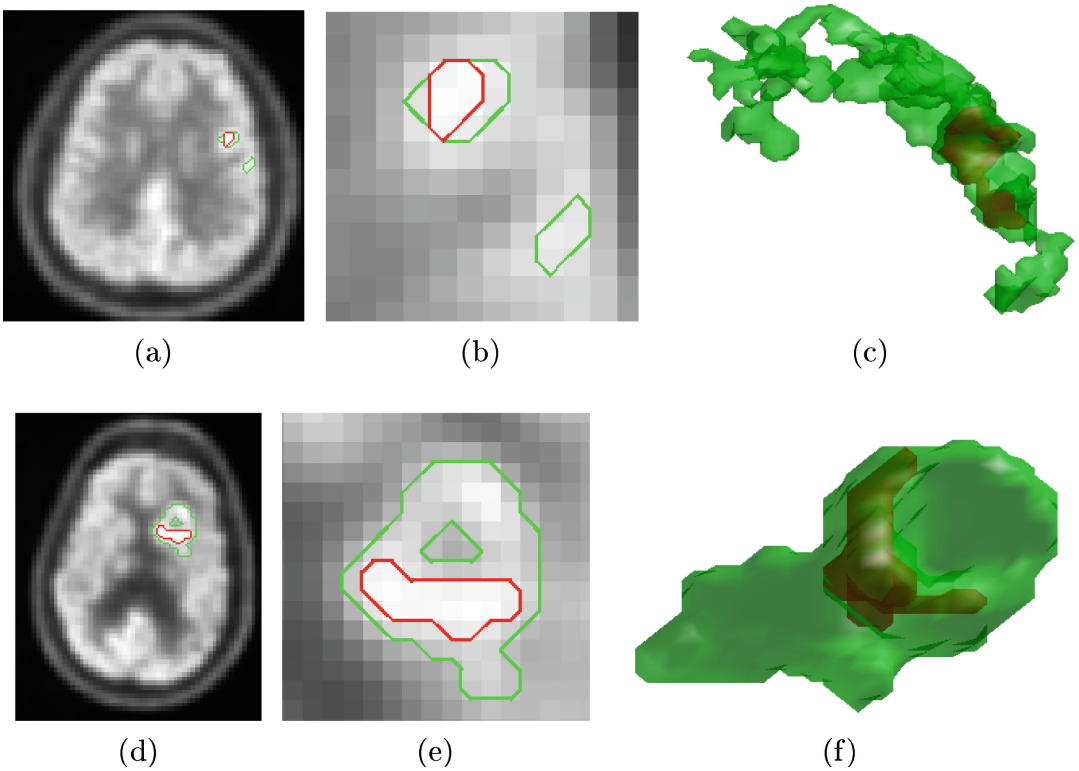

Fig. 4. Evaluation of the criterion χ_t for P2 (first row) and P5 (second row): comparison between the true positive lesions detected with (in red) or without (in green) previously applying the criterion χ_t. Results shown on a PET slice ((a) and (d)) zoomed in (b) and (e), and in 3D ((c) and (f)). (Color figure online)

The detection performance was characterized using the True Positive Rate (TPR), defined as the ratio between the number of true tumors among the detected lesions and the real number of tumors, and the Positive Predictive Value (PPV), defined as the ratio between the number of true tumors among the detected lesions and the total number of detected lesions. The true tumors were defined as the detected tumors having a non empty intersection with the ground truth. As shown by the TPR in Table 1, the algorithm detected all the lesions visible in the PET images. As shown by the PPV in Table 1, the algorithm also detected false positives, but drastically less after using topological and symmetry information in a post-processing (PP) step.

The usefulness of the PP was also assessed visually. As shown in Fig. 3b, the PP eliminates false positives due to the physiological uptake of symmetrical structures such as basal nuclei. The remaining false positives are due to other asymetrical physiological uptake in the brain (Fig. 3c).

Moreover, applying the criterion χ_t before the spatial context criterion χ_c prevents the true detected lesions from merging with basal nuclei (Fig. 4c) or other brain physiological uptake regions (Fig. 4f). However, as previously shown

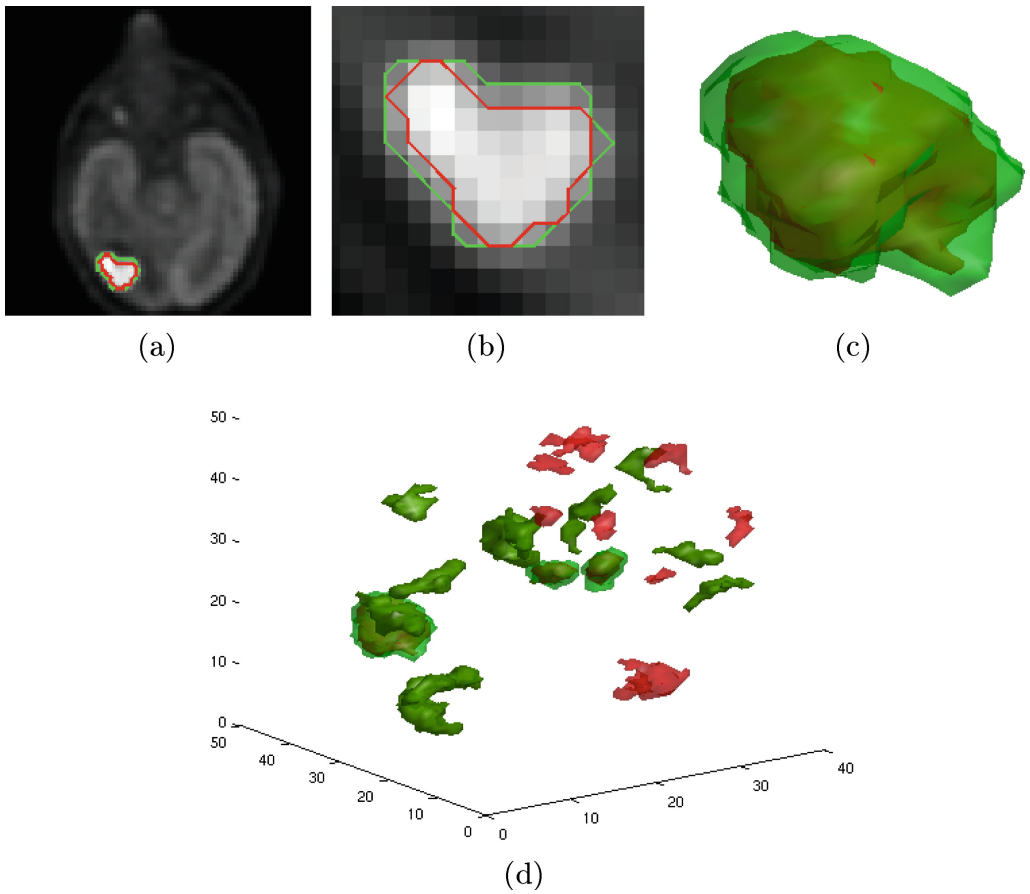

Fig. 5. Influence of the spatial context parameter s for P4: comparison between the detection setting $s = 1$ (in green) and $s = 5$ (in red). Results shown on a PET slice (a), zoomed in (b), and in 3D for only the true positive (c) or all the detected lesions before PP (d). (Color figure online)

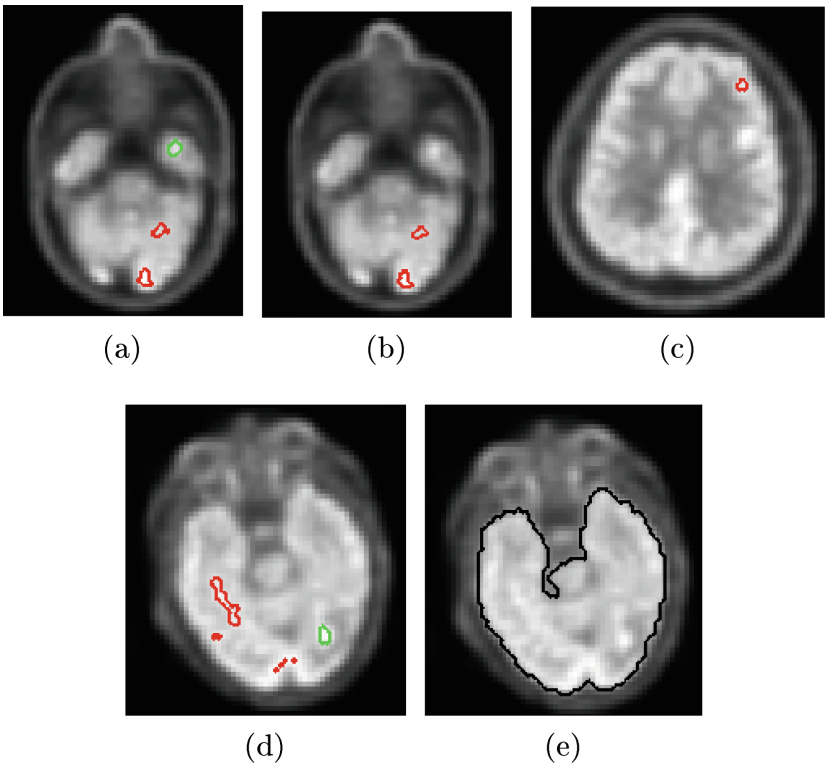

Fig. 6. Influence of the parameters K_c^1, K_c^2 and K_t: comparison between the detected lesions, true (in green) or false (in red) positives. Results shown on PET slices setting $K_c^2 = 4$ (a) or $K_c^2 = 5$ (b) for P3, $K_t^1 = 1$ for P2 (c), $K_c^1 = 1$ for P1 with (d) or without (e) previously applying the criterion χ_t. (Color figure online)

in Fig. 3b, applying χ_t does not reduce the detected volume for tumors isolated from physiological radiotracer uptake.

The influence of the spatial context parameter s value was also tested. As shown in Fig. 5 increasing the s value still allows detecting the actual lesion, but reduces its volume and increases the number of false positives.

Finally, the influence of the other parameters K_c^1, K_c^2 and K_t were tested. As shown in Fig. 6, increasing K_c^2 or K_t can prevent the algorithm from detecting too small tumors. Modifying the K_c^1 value has no effect on the detection (Fig. 6d). However, the result is different if the criterion χ_t is not previously applied (Fig. 6e where the whole brain is detected), which shows that applying χ_t also penalizes too large nodes.

4 Discussion and Conclusion

In this paper, we proposed a method based on a 3D max-tree representation and a new selection criterion based on the spatial context to detect brain lesions on 3D PET images. Our algorithm identifies tumor locations, preventing the detected lesions from merging with spatially close physiological uptake regions, at the price of a final reduced tumor volume. Thus, it is intended to be a detection method that can serve as a preliminary step for a segmentation method, such

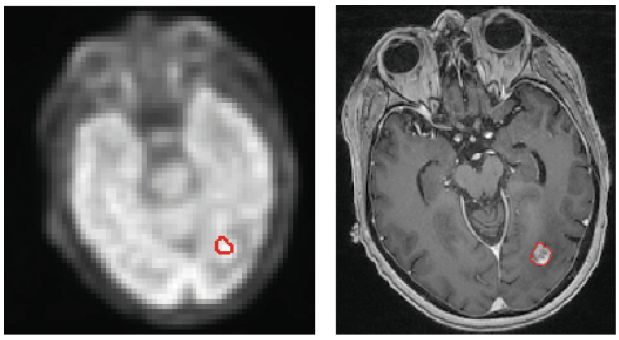

(a) (b)

Fig. 7. Results of a MR segmentation method initialized with the PET for P1. (a) Superimposing of the PET image on the contours of the detected lesion (in red). (b) Superimposing of the MR image on the contours of the segmented lesion (in red). (Color figure online)

as the one described in [3] to segment brain tumors on MR images in a variational approach using information from the PET (Fig. 7). However, the proposed method still detects asymetrical areas of physiological increased uptake, which could be further removed in our approach using complementary information from MRI volumes. Moreover, using MRI allows detecting other lesions, not visible in the ^{18}F-FDG PET, which is not the standard imaging procedure for metastasis diagnosis. Thus, our detection algorithm depends on the quality of the information given by the PET image. Finally, our method can also be extended to other brain lesions as shown in [12].

Acknowledgments. This work was supported by the "Lidex-PIM" project funded by the IDEX Paris-Saclay, ANR-11-IDEX-0003-02.

References

1. Foster, B., Bagci, U., Mansoor, A., Xu, Z., Mollura, D.J.: A review on segmentation of positron emission tomography images. Comput. Biol. Med. **50**, 76–96 (2014)
2. Bagci, U., Udupa, J.K., Mendhiratta, N., Foster, B., Xu, Z., Yao, J., Chen, X., Mollura, D.J.: Joint segmentation of anatomical and functional images: applications in quantification of lesions from PET, PET-CT and MRI-PET-CT images. Med. Image Anal. **17**, 929–945 (2013)
3. Urien, H., Buvat, I., Rougon, R., Boughdad, S., Bloch, I.: PET-driven multi-phase segmentation on meningiomas in MRI. In: IEEE International Symposium on Biomedical Imaging (ISBI), pp. 407–410 (2016)
4. Salembier, P., Oliveras, A., Garrido, L.: Antiextensive connected operators for image and sequence processing. IEEE Trans. Image Process. **7**(4), 555–570 (1998)
5. Carlinet, E., Géraud, T.: A comparative review of component tree computation algorithms. IEEE Trans. Image Process. **23**(9), 3885–3895 (2014)
6. Salembier, P., Wilkinson, M.H.F.: Connected operators. IEEE Sig. Process. Mag. **26**(6), 136–157 (2009)

7. Grossiord, E., Talbot, H., Passat, N., Meignan, M., Tervé, P., Najman, L.: Hierarchies and shape-space for PET image segmentation. In: IEEE International Symposium on Biomedical Imaging (ISBI), pp. 1118–1121 (2015)
8. Xu, Y., Géraud, T., Najman, L.: Context-based energy estimator: application to object segmentation on the tree of shapes. In: IEEE International Conference on Image Processing, pp. 1577–1580 (2012)
9. Boellaard, R., ODoherty, M.J., Weber, W.A., Mottaghy, F.M., Lonsdale, M.N., Stroobants, S.G., Oyen, W.J.G., Kotzerke, J., Hoekstra, O.S., Pruim, J., et al.: FDG PET and PET/CT: EANM procedure guidelines for tumour PET imaging: version 1.0. Eur. J. Nucl. Med. Mol. Imaging **37**(1), 181–200 (2010)
10. Otsu, N.: A threshold selection method from gray-level histograms. Automatica **11**, 285–296 (1975)
11. Tuzikov, A.V., Colliot, O., Bloch, I.: Evaluation of the symmetry image plane in 3D MR brain images. Pattern Recogn. Lett. **24**(14), 2219–2233 (2003)
12. Urien, H., Buvat, I., Rougon, N., Bloch, I.: A 3D hierarchical multimodal detection and segmentation method for multiple sclerosis lesions in MRI. In: MICCAI Multiple Sclerosis SEGmentation (MSSEG) Challenge, pp. 69–74 (2016)